The third Moscow Solar System Symposium (3M-S^3)
Moscow 2012

FULL TOPOGRAPHIC CORRECTION OF M³ REFLECTANCE DATA FOR LUNAR ELEMENTAL ABUNDANCE ESTIMATION

A. Grumpe[1], C. Wöhler[1], A. Berezhnoy[2], *[1]Image Analysis Group, TU Dortmund University, Otto-Hahn-Str. 4, 44227 Dortmund, Germany; [2]Sternberg Astronomical Institute, Moscow State University, Universitetskij pr. 13, Moscow, Russia. Contact: {arne.grumpe | christian.woehler}@tu-dortmund.de, ber@sai.msu.ru*

Introduction: In lunar remote sensing, the composition of the surface is commonly derived from the observed reflectance spectra. The normalisation of the surface reflectance to a reference illumination and viewing geometry (commonly: 30° incidence angle, 0° emission angle, 30° phase angle [1]) requires knowledge of the small-scale topography, since without topographic correction significant residual distortions of the spectra tend to occur [2]. Accordingly, insufficient topographic correction leads to topography-related artifacts in metal oxide abundance maps inferred from multispectral imagery [3]. However, the best currently available global lunar digital elevation models (DEMs), the LOLA DEM [4] and the GLD100 [5], have a much lower effective lateral resolution than the M³ image data, the currently best-resolved lunar hyperspectral data set (140 m/pixel in global mode [6]). In this study we therefore describe a framework for the correction of M³ reflectance data with respect to topography on both large and small spatial scales and the estimation of elemental abundances.

Image registration and DEM construction: We apply the photometric stereo based method proposed in [7] to M³ radiance data and a reference DEM (here: the GLD100) of lower lateral resolution than the images. Our method relies on an estimation of the surface gradients by simultaneously minimising the mean squared deviation between the observed reflectances and those expected from the constructed DEM, and the mean squared deviation of the large-scale gradients of the constructed DEM from those of the reference DEM. For DEM construction, only M³ channels with centre wavelengths below 2000 nm are used in order to avoid the thermal emission component. The Hapke model [8] is used as the reflectance function, where the single-particle scattering function is chosen according to the double-lobed form proposed in [9] which is governed by a single asymmetry parameter. Along with the DEM, our approach performs a pixel-wise estimation of the single-scattering albedo and (if two or more images acquired under sufficiently different phase angles are available) the asymmetry parameter. The remaining Hapke parameters describing the opposition effect (which is negligible for the regarded range of phase angles) and the macroscopic surface roughness are chosen according to [10].

Our photometric stereo method is applicable using a single image, but it yields a higher accuracy when several pixel-synchronous images acquired under different illumination conditions are available. The M³ images, however, show misregistrations of up to several kilometers, which might be due to failure of the navigational instruments of Chandrayaan-1 and the resulting problems of M³ selenelocation [11]. Image registration is further complicated by strongly varying illumination conditions during different orbits. Because of the changing illumination and the resulting intensity changes, similarity measures like cross-correlation fail on the M³ images. In contrast, the photometrically reconstructed surface gradients are an illumination-independent representation of the images. Thus, by matching control points (e.g. corner points) of the surface gradient images using cross-correlation, illumination independence is achieved [7].

Spectral parameters, elemental abundances: The thermal emission component is subtracted from the M³ radiance spectra [2]. For each M³ channel, a pixel-wise estimation of the single-scattering albedo and the asymmetry parameter is performed based on the Hapke model [8], relying on the available M³ images and the constructed DEM. The Hapke model [8] is then used to determine the surface reflectance for the (30°, 0°, 30°) reference geometry. Normalised reflectance data of our test region (the crater Aristillus) downloaded from [11] and obtained using our method, respectively, are shown in Fig. 1. Due to the high lateral resolution of our DEM, all topography-related artifacts have been removed from the normalised reflectances. Our DEM of Aristillus is shown in Fig. 2. For each pixel, the continuum of the reflectance spectrum is then removed based on the convex hull [12], which also yields the continuum slopes for the absorption troughs around 1000 nm and 2000 nm. The absorption wavelength, depth, and width of both absorption troughs are determined based on the continuum-removed spectra [2] (cf. Fig. 3). We used global maps of these parameters at a resolution of 0.2 pixels per degree to determine a linear regression model based on the Lunar Prospector elemental abundance maps of the elements Ca, Al, Fe, Mg, Ti, and O [13] (cf. Fig. 4). This regression model allows to construct high-resolution elemental abundance maps along with a petrographic map in terms of the three-endmember model [14] using the spectral parameter maps obtained at full M³ resolution (cf. Fig. 5).

Summary and conclusion: We have described the determination of reflectance data normalised to a reference geometry based on lunar DEMs of high lateral resolution constructed using a photometric stereo based method. The normalised reflectances as well as the inferred spectral parameters are free of topography-related artifacts. The obtained spectral parameter maps have been used for the estimation of elemental abundances.

References: [1] Pieters, C. M. (1999) Workshop New Views of the Moon 2, 47. [2] Wöhler, C. and Grumpe, A. (2012) In: Innovations for Shape Analysis: Models and Algorithms. Rev. contrib. to Dagstuhl Seminar, Springer, to appear. [3] Jolliff, B. L. (1999). JGR 104(E6), 14123–14148. [4] Li, R. et al. (2011) LPSC XXXXII, abstract #2010. [5] Scholten, F., et al. (2011) LPSC XXXXII, abstract #2046. [6] Pieters, C. M., et al. (2009) Current Science 96(4), 500–505. [7] Grumpe, A. and Wöhler, C. (2011) Proc. 7th IEEE Int. Symp. Image and Signal Proc. and Anal., 609–614. [8] Hapke, B. W. (2002) Icarus 157, 523–534. [9] Cornette, W. M. and Shanks, J. G. (1992) Appl. Optics 31(16), 3152–3160. [10] Warell, J. (2004) Icarus 167, 271–286. [11] Boardman, J. W., et al. (2011) JGR 116, E00G14. [12] Fu, Z., et al. (2007) IEEE Trans. Geoscience and Remote Sensing 45(11), 3827–3844. [13] Wöhler, C., et al. (2011) PSS 59, 92–110. [14] Berezhnoy, A. A., et al. (2005) PSS 53, 1097–1108. [15] http://pds-imaging.jpl.nasa.gov/volumes/m3.html. [16] Wiseman, S. M., et al. (2012) Proc. 2nd Conf. Lunar Highlands Crust, abstract #9025. [17] http://www.mapaplanet.org/explorer/moon.html.

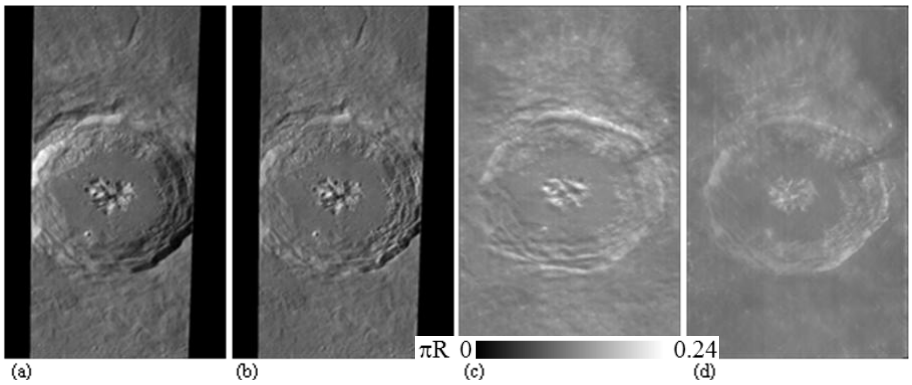

Fig. 1: (a) M³ 1579 nm radiance image of Aristillus at 57.9° phase angle. (b) and (c) M³ 1579 nm reflectance normalised to (30°, 0°, 30°) standard geometry, inferred from images acquired at phase angles of 57.9° and 38.8°, with topographic correction based on the LOLA DEM (from [15]). (d) M³ 1579 nm reflectance normalised to (30°, 0°, 30°) with full topographic correction. Images (b), (c), and (d) are scaled to the same reflectance range.

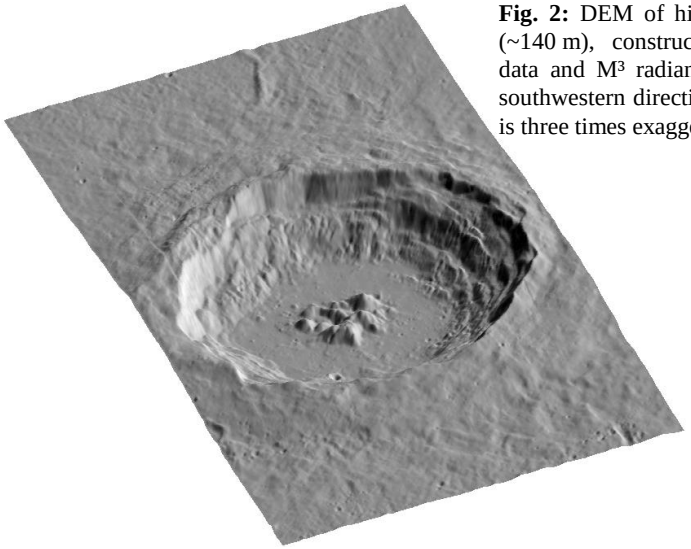

Fig. 2: DEM of high lateral resolution (~140 m), constructed using GLD100 data and M³ radiance data. View from southwestern direction. The vertical axis is three times exaggerated.

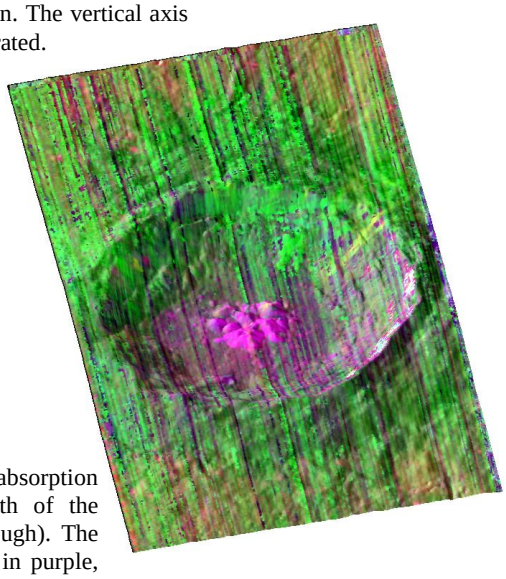

Fig. 3: Map of spectral parameters overlaid on the DEM (R channel: absorption depth of the ~1000 nm trough; G channel: absorption wavelength of the ~1000 nm trough; B channel: absorption depth of the ~2000 nm trough). The presumably noritic central peaks (low absorption wavelength) appear in purple, the olivine streaks on the northeastern crater wall (cf. [16]) (high absorption wavelength, nearly absent absorption at ~2000 nm) in yellow colour.

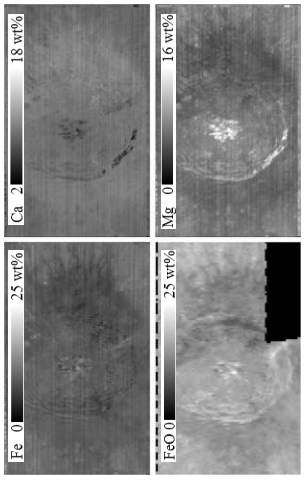

Fig. 4: Abundances of Ca (upper left), Mg (upper right), and Fe (lower left). For comparison, the Clementine FeO abundance map obtained from [17] is shown on the lower right, where the influence of topography is clearly apparent.

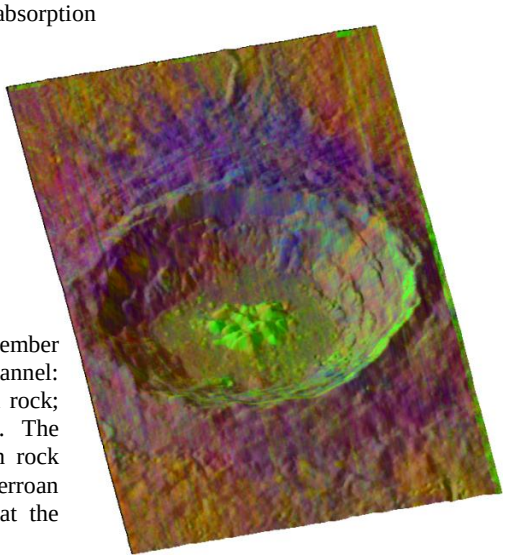

Fig. 5: Petrographic three-endmember map overlaid on the DEM. R channel: mare basalt; G channel: Mg-rich rock; B channel: ferroan anorthosite. The central peaks consist of Mg-rich rock (presumably norite), and a large ferroan anorthosite deposit is apparent at the northern crater wall and rim.